Monthly Notices
of the
ROYAL ASTRONOMICAL SOCIETY

MNRAS **487,** 919–927 (2019)
Advance Access publication 2019 May 14

doi:10.1093/mnras/stz1312

HD 226766: a hierarchical SB3 system with two twin Am stars

G. Catanzaro [1]★ M. Gangi,[2] M. Giarrusso [3] M. Munari[1] and F. Leone [1,2]

[1]*INAF-Osservatorio Astrofisico di Catania, Via S. Sofia 78, I-95123, Catania, Italy*
[2]*Universitá degli studi di Catania, Via S. Sofia 78, I-95123, Catania, Italy*
[3]*INFN Laboratori Nazionali del Sud, Via S. Sofia 62, I-95123, Catania, Italy*

Accepted 2019 May 8. Received 2019 May 8; in original form 2019 February 20

ABSTRACT

In this paper, we present a detailed revision of the orbital parameters and the first quantitative abundance analysis of the spectroscopic triple system HD 226766. By means of a simultaneous fit of the radial velocities of all the three components, we derived precise orbital parameters for the system, in particular inner pair has $P(\mathrm{d}) = 31.9187 \pm 0.0001$, $e = 0.28 \pm 0.01$, and $M_\mathrm{A}/M_\mathrm{B} = 1.03 \pm 0.03$, while the C component orbits around the inner pair with a period of $P(\mathrm{d}) = 1615 \pm 59$ in a very eccentric orbit ($e = 0.54 \pm 0.11$). From the fit of the Hβ and Hα profiles, we determined the effective temperatures and surface gravities of each component of the inner pair: $T_\mathrm{eff} = 8600 \pm 500$ K and $\log g = 3.8 \pm 0.2$ for HD 226766 A and $T_\mathrm{eff} = 8500 \pm 400$ K and $\log g = 4.0 \pm 0.2$ for HD 226766 B. In the hypothesis that component C is a main sequence star ($\log g = 4.0$) we derived $T_\mathrm{eff} = 8000 \pm 500$ K. Rotational velocities have been estimated by modeling the profiles of metallic lines: $v \sin i = 13 \pm 1$ km s^{-1} for inner pair and $v \sin i = 150 \pm 20$ km s^{-1} for the C component. We find that the inner pair is heterogeneous from the point of view of the chemical composition: both stars are very similar and show chemical anomalies typical of Am stars. With some hypothesis about the masses of the components, we estimated the orbital inclination angle for the inner binary, $i = (47 \pm 1)^\circ$, and for the outer orbit, $i = (54 \pm 19)^\circ$.

Key words: Stars: abundances – (stars:) binaries: spectroscopic – Stars: chemically peculiar – Stars: early-type – Stars: individual: HD 226766.

1 INTRODUCTION

The peculiar nature of HD 226766 (= KIC 5219533) as Am star was first reported by Renson & Manfroid (2009), who classified it as an A2-A8 star with a companion. Am stars show Ca II K-line too early for their hydrogen line types, while lines generated by iron-peak elements appear too late, such that the spectral types inferred from the Ca II K- and metal lines could differ by five or more spectral sub-classes. The typical chemical pattern shows underabundances of Ca and/or Sc and overabundances of the Fe-peak elements, Y, Ba, and rare earths elements (Catanzaro & Balona 2012; Catanzaro, Ripepi & Bruntt 2013; Catanzaro & Ripepi 2014; Catanzaro et al. 2015). This star forms a visual double system with the single-lined spectroscopic binary (SB1) star HD 189178 (Leone & Catanzaro 1999).

HD 226766 has been observed two times by LAMOST in the framework of the 'LAMOST-Kepler project' (De Cat et al. 2015). LAMOST spectra have been analyzed by Frasca et al. (2016) in order to derive atmospheric parameters including effective temperatures, gravities, and metallicities. For all the stars with more than one observation, following Press et al. (1992), these authors computed the χ^2 probability that radial velocity variation has a random occurrence. In the case of our target, this probability is low ($P(\chi^2) = 0.313$), confirming that the star is probably a tru e binary.

According to these evidences, this object was inserted in our ongoing spectroscopic monitoring of suspected Chemically Peculiar stars selected from Renson & Manfroid (2009) (see for details Catanzaro et al. 2019). Preliminary results of this study have been presented by Catanzaro (2017), who first focus the attention on the possible presence of a third companion orbiting around the inner SB2 pair. Catanzaro (2017) found a period of 31.915 d, an eccentricity of the orbit of 0.29, and a mass ratio of 1.04 for the inner pair, while the third star orbits around their centre of mass with a period of 970 d.

Recently, Lampens et al. (2018) performed a spectroscopic analysis on a sample of A-F hybrid stars discovered by Kepler, deriving orbital parameters and some atmospheric proprieties. In particular, for HD 226766 they confirmed the presence of a more rapidly rotating third component of a slightly cooler spectral type and derived orbital parameters for the inner pair, in agreement with the preliminary results of Catanzaro (2017). Regarding the nature of these components, they concluded that it is composed of two nearly

★ E-mail: giovanni.catanzaro@inaf.it

identical stars with $T_{\rm eff} \approx 8300$ K and revolving with a period of 31.9181 ± 0.0006 d in an orbit with an eccentricity of 0.27. They have also tried to characterize the outer orbit with a period of about 1600 d and $e = 0.57$.

Later on, Murphy et al. (2018) studied this multiple system by using phase modulation method (Murphy et al. 2014). They found this system to have a very high mass function and, according to their analysis, the third body should be a δ Sct star with an orbital period > 1500 d.

The purpose of this paper is then twofold: first of all, give a complete characterization of both the inner and outer orbits of the HD 226766 system, and then to perform an accurate spectroscopic investigation about the chemical composition of the system components.

2 OBSERVATIONS AND DATA REDUCTION

Spectroscopic observations of HD 226766 (listed in Table 1) were carried out with the Catania Astrophysical Observatory Spectropolarimeter (CAOS) which is a fibre-fed, high-resolution, cross-dispersed echelle spectrograph (Leone et al. 2016) installed at the Cassegrain focus of the 91 cm telescope of the 'M. G. Fracastoro' observing station of the Catania Astrophysical Observatory (Mt Etna, Italy).

Our spectra were obtained between 2014 September and 2018 December. Exposure times have been tuned in order to obtain for the stars a signal-to-noise ratio of at least 60 in the continuum in the 3900−6800 Å spectral range, with a resolution of $R = 45\,000$, as measured from ThAr and telluric lines.

The reduction of all spectra, which included the subtraction of the bias frame, trimming, correcting for the flat-field and the scattered light, extraction of the orders, and wavelength calibration, was done using the NOAO/IRAF packages. Given the importance of Balmer lines in our analysis, we paid much more attention to the normalization of the corresponding spectral orders. In particular, we divided the spectral order containing Hα and Hβ by a pseudo-continuum obtained combining the continua of the previous and subsequent echelle orders, as already outlined by Catanzaro et al. (2015). The IRAF package *rvcorrect* was used to determine the barycentric velocity and correct the observed radial velocities for the Earth's motion.

The radial velocities of HD 226766 A and HD 226766 B, reported in Table 1, have been measured by cross-correlating each observed spectrum with a synthetic template computed with the parameters derived in Section 4. The cross-correlation has been calculated by means of the IRAF task *fxcor* excluding Balmer lines as well as intervals with telluric lines. Velocities of centre of mass of this pair have been derived as

$$Vr_\gamma = \frac{Vr_{\rm A} + Vr_{\rm B}}{2} \tag{1}$$

and are reported in Table 1.

3 ORBITAL SOLUTION

The radial velocities for a spectroscopic binary system are given from the following equation:

$$V_{\rm rad} = \gamma + K[\cos(\theta + \omega) + e\cos\omega] \tag{2}$$

where γ is the radial velocity of the centre of mass, e is the eccentricity of the orbit, ω is the longitude of the periastron, θ is the angular position of the star measured from the centre of mass at a given instant, the so-called true anomaly, and K is the semi-amplitude of the velocity curve as given by the formula:

$$K = \frac{2\pi a \sin i}{P\sqrt{1-e^2}} \tag{3}$$

where P is the orbital period of the system.

In order to derive a simultaneous solution for the triple system, orbital elements have been determined by a weighted least squares fitting to equation (2), where instead of a constant value of γ we considered a variable velocity with the same analytic form of equation (2). Errors have been estimated as the variation in the parameters that increases the χ^2 of a unit. To improve the precision of our solution, we considered also the radial velocities published by Lampens et al. (2018).

The starting value for the orbital period $P = 31.9080 \pm 0.0006$ d, was evaluated using the Phase Dispersion Method (Stellingwerf 1978) as coded in the NOAO/IRAF package. The radial velocities folded with this period are displayed in Fig. 1. The extreme dispersion of the data, as already reported in Catanzaro (2017), is the first argument in favour of the presence of a third body revolving around the inner SB2 pair.

The result of this procedure is shown in Fig. 2, where we plotted radial velocities versus julian date with overplotted theoretical curves computed with the orbital parameters reported in Table 2. In Fig. 3 we show the radial velocities for the SB2 system after correcting them for the motion of the centre of mass of the system. The near-unity value of the mass ratio confirms the Lampens et al. (2018) hypothesis that the stars are very similar. In Fig. 4, we plotted our solution for the outer orbit of HD 226766 C.

All these results, both for the inner pair and for the outer orbit, are in agreement with those of Lampens et al. (2018).

4 ATMOSPHERIC PARAMETERS

One of the methods commonly used to determine effective temperature ($T_{\rm eff}$) and surface gravity ($\log g$) of a star is to compare the observed and theoretical profiles of Balmer lines; see for instance Catanzaro et al. (2015), Catanzaro & Ripepi (2014), Catanzaro et al. (2013), and Catanzaro & Balona (2012). In the case of our system, we observed Hβ and Hα profiles given by the superposition of lines Doppler-shifted by the orbital motion. The fitting procedure has been already applied by us in other study of binary and multiple systems (see for instance Catanzaro & Leone 2006; Catanzaro 2010).

Lampens et al. (2018) found $T_{\rm eff}^A = 8300 \pm 100$ K and $T_{\rm eff}^B = 8200 \pm 100$ K. We used these values as starting guesses for an iterative procedure aimed at minimizing the difference between observed and synthetic spectra, using as goodness-of-fit parameter the χ^2 defined as

$$\chi^2 = \frac{1}{N}\sum_\lambda \left(\frac{I_{\rm obs} - I_{\rm th}}{\delta I_{\rm obs}}\right)^2 \tag{4}$$

where N is the total number of points, $I_{\rm obs}$ and $I_{\rm th}$ are the intensities of the observed and computed profiles, respectively, and $\delta I_{\rm obs}$ is the root mean square of the photon noise. Synthetic spectra for both components were generated in three steps: (i) we computed LTE atmospheric models using the ATLAS9 code (Kurucz 1993, 1993b); (ii) the stellar spectra were synthesized using SYNTHE (Kurucz & Avrett 1981); and (iii) the spectra were convolved for the instrumental and rotational broadening. In particular, we determined the $v\sin i$ of our target by matching synthetic lines profiles from SYNTHE to a set of metal lines, in particular the Mg I triplet at

Table 1. Radial velocities derived for the component of the inner pair of the HD 226766 system and for its centre of mass.

HJD (2400000. +)	Vr_A km s^{-1}	Vr_B km s^{-1}	$Vr\gamma$ km s^{-1}	HJD (2400000. +)	Vr_A km s^{-1}	Vr_B km s^{-1}	$Vr\gamma$ km s^{-1}
56912.4411	− 22.12 ± 0.39	50.10 ± 0.53	14.0 ± 0.7	57337.3744	31.04 ± 0.84	− 24.72 ± 0.98	3.1 ± 1.3
56932.3207	24.10 ± 0.45	− 0.73 ± 0.54	11.7 ± 0.7	57338.3508	44.07 ± 0.42	− 37.05 ± 0.61	3.5 ± 0.7
56933.2809	11.53 ± 0.40	11.53 ± 0.40	11.5 ± 0.6	57340.2441	61.00 ± 0.51	− 55.63 ± 0.66	2.7 ± 0.8
56938.3788	− 13.25 ± 0.37	36.34 ± 0.56	11.5 ± 0.7	57346.3526	23.58 ± 2.98	− 17.28 ± 3.76	3.1 ± 2.8
56941.3303	− 21.40 ± 0.58	44.72 ± 0.75	11.6 ± 0.9	57567.5476	45.96 ± 0.38	− 34.76 ± 0.56	5.6 ± 0.7
56943.3503	− 23.70 ± 0.49	47.47 ± 0.64	11.9 ± 0.8	57570.5231	17.88 ± 0.68	− 8.18 ± 0.76	4.8 ± 1.0
56944.3017	− 24.67 ± 0.43	47.36 ± 0.56	11.3 ± 0.7	57574.5300	− 8.46 ± 0.36	20.79 ± 0.53	6.2 ± 0.6
56945.3798	− 23.63 ± 0.91	47.16 ± 1.07	11.8 ± 1.4	57577.5227	− 21.97 ± 4.93	32.33 ± 5.82	5.2 ± 2.6
56946.3438	− 24.73 ± 0.52	44.11 ± 0.65	9.7 ± 0.8	57581.5433	− 29.78 ± 0.46	40.90 ± 0.60	5.6 ± 0.8
56948.3697	− 17.97 ± 0.70	40.27 ± 0.94	11.1 ± 1.1	57587.5779	− 18.21 ± 0.46	31.83 ± 0.59	6.8 ± 0.7
56949.2909	− 14.52 ± 0.33	35.52 ± 0.49	10.5 ± 0.6	57597.5051	60.47 ± 0.33	− 52.01 ± 0.41	4.2 ± 0.5
56961.3907	46.66 ± 0.67	− 28.21 ± 0.85	9.2 ± 1.1	57603.4384	5.69 ± 0.15	5.69 ± 0.15	5.7 ± 0.2
56980.2873	− 20.61 ± 0.47	37.48 ± 0.65	8.4 ± 0.8	57610.5053	− 23.85 ± 0.54	37.54 ± 0.64	6.8 ± 0.8
57197.5955	− 30.73 ± 0.41	37.85 ± 0.49	3.5 ± 0.6	57611.5233	− 26.22 ± 0.54	39.00 ± 0.97	6.4 ± 1.1
57203.5711	− 24.38 ± 0.36	34.54 ± 0.48	5.1 ± 0.6	57626.4355	55.58 ± 0.67	− 45.49 ± 0.80	5.0 ± 1.0
57204.5822	− 20.70 ± 0.35	29.65 ± 0.49	4.5 ± 0.6	57635.3522	4.16 ± 0.24	4.16 ± 0.24	4.2 ± 0.3
57207.5955	5.92 ± 0.13	5.92 ± 0.13	5.9 ± 0.2	57666.3311	18.65 ± 0.58	− 5.86 ± 0.72	6.4 ± 0.9
57220.5143	4.67 ± 0.16	4.67 ± 0.16	4.7 ± 0.2	57677.5325	− 28.49 ± 0.44	43.64 ± 0.56	7.6 ± 0.7
57234.5562	− 28.27 ± 0.46	36.04 ± 0.56	3.9 ± 0.7	57680.5349	− 26.20 ± 0.39	41.79 ± 0.51	7.8 ± 0.6
57255.5988	− 11.65 ± 0.48	19.31 ± 0.69	3.8 ± 0.8	57919.5668	42.25 ± 0.41	− 20.36 ± 0.48	10.9 ± 0.6
57256.4927	− 16.11 ± 0.41	24.33 ± 0.58	4.1 ± 0.7	57920.5782	32.10 ± 0.41	− 12.77 ± 0.47	9.7 ± 0.6
57257.5085	− 20.43 ± 1.67	28.01 ± 2.02	3.8 ± 2.6	57933.5276	− 24.46 ± 0.44	47.78 ± 0.55	11.7 ± 0.7
57259.4092	− 25.63 ± 0.39	35.02 ± 0.50	4.7 ± 0.6	57934.5253	− 24.61 ± 0.40	47.27 ± 0.55	11.3 ± 0.7
57260.4250	− 28.50 ± 0.40	36.63 ± 0.50	4.1 ± 0.6	57935.5471	− 24.35 ± 0.48	45.31 ± 0.61	10.5 ± 0.8
57261.4622	− 28.76 ± 0.51	39.82 ± 0.62	5.5 ± 0.8	57940.5125	− 1.70 ± 0.41	21.01 ± 0.56	9.6 ± 0.7
57262.4843	− 30.13 ± 0.66	40.42 ± 0.77	5.1 ± 1.0	57941.5045	9.83 ± 0.17	9.83 ± 0.17	9.8 ± 0.2
57263.4402	− 31.41 ± 0.43	40.07 ± 0.51	4.3 ± 0.7	57959.4892	− 12.83 ± 0.51	35.77 ± 0.68	11.5 ± 0.8
57264.3935	− 30.74 ± 0.43	40.32 ± 0.51	4.8 ± 0.7	57962.4613	− 21.97 ± 0.56	43.53 ± 0.74	10.8 ± 0.9
57269.3841	− 14.22 ± 0.36	24.14 ± 0.49	5.0 ± 0.6	57993.4039	− 18.94 ± 0.34	42.13 ± 0.47	11.6 ± 0.6
57271.3825	3.57 ± 0.22	3.57 ± 0.22	3.6 ± 0.3	58002.3626	− 14.77 ± 0.35	37.11 ± 0.52	11.2 ± 0.6
57272.4131	15.51 ± 0.66	− 8.47 ± 0.71	3.5 ± 1.0	58011.3477	70.88 ± 0.43	− 48.85 ± 0.60	11.0 ± 0.7
57276.3819	61.45 ± 0.57	− 55.15 ± 0.75	3.1 ± 0.9	58046.2661	51.71 ± 0.41	− 28.61 ± 0.55	11.5 ± 0.7
57277.3651	62.53 ± 0.42	− 57.20 ± 0.58	2.7 ± 0.7	58102.2363	27.11 ± 0.59	1.83 ± 0.68	14.5 ± 0.9
57278.3616	58.66 ± 0.48	− 53.96 ± 0.65	2.3 ± 0.8	58270.6031	53.76 ± 0.88	− 10.06 ± 1.01	21.8 ± 1.3
57279.3761	50.94 ± 0.56	− 46.78 ± 0.82	2.1 ± 1.0	58277.5863	3.54 ± 0.90	42.43 ± 0.03	23.0 ± 0.9
57280.3527	43.04 ± 1.08	− 36.29 ± 1.52	3.4 ± 1.9	58291.5577	10.98 ± 0.48	36.04 ± 0.61	23.5 ± 0.8
57281.3490	33.32 ± 0.42	− 26.87 ± 0.55	3.2 ± 0.7	58298.5284	84.71 ± 0.39	− 34.39 ± 0.52	25.2 ± 0.6
57282.3662	24.76 ± 0.50	− 17.92 ± 0.59	3.4 ± 0.8	58299.5306	79.57 ± 0.39	− 33.38 ± 0.49	23.1 ± 0.6
57283.3589	15.65 ± 0.40	− 8.82 ± 0.45	3.4 ± 0.6	58305.5159	35.80 ± 0.31	23.60 ± 0.31	29.7 ± 0.4
57284.3235	4.33 ± 0.18	4.33 ± 0.18	4.3 ± 0.2	58306.5449	22.52 ± 0.12	22.52 ± 0.12	22.5 ± 0.2
57286.3291	− 5.08 ± 0.33	13.13 ± 0.50	4.0 ± 0.6	58311.5645	− 4.09 ± 0.39	51.87 ± 0.52	23.9 ± 0.6
57288.3653	− 15.21 ± 0.39	24.74 ± 0.55	4.8 ± 0.7	58312.5243	− 6.31 ± 0.33	54.98 ± 0.46	24.3 ± 0.6
57290.3208	− 23.30 ± 0.35	31.34 ± 0.47	4.0 ± 0.6	58319.6112	− 8.70 ± 0.88	58.10 ± 2.34	24.7 ± 2.5
57302.3759	− 7.38 ± 0.40	12.86 ± 0.60	2.7 ± 0.7	58330.5082	84.10 ± 0.48	− 35.43 ± 0.64	24.3 ± 0.8
57307.2926	53.12 ± 0.43	− 48.85 ± 0.61	2.1 ± 0.7	58336.4468	42.21 ± 0.58	16.14 ± 0.68	29.2 ± 0.9
57308.3377	60.91 ± 0.39	− 56.61 ± 0.53	2.1 ± 0.7	58337.4354	29.51 ± 0.34	29.51 ± 0.34	29.5 ± 0.5
57309.3764	62.45 ± 0.66	− 57.42 ± 0.92	2.5 ± 1.1	58367.4017	51.98 ± 0.44	6.00 ± 0.62	29.0 ± 0.8
57336.3710	18.17 ± 0.46	− 8.91 ± 0.59	4.6 ± 0.7	58476.2074	− 17.12 ± 1.37	54.84 ± 2.30	18.8 ± 2.7

λλ5167-5183 Å. The best fit occurs for a $v \sin i = 13 \pm 1$ km s^{-1} for each of the two components.

Finally, since the dynamical masses are equal within errors for both inner components, the same radius has been assumed and therefore, following Catanzaro & Leone (2006) and Catanzaro (2010), single synthetic spectra have been combined to obtain the composite synthetic spectrum normalized to the continuum level by following the formula:

$$F_{\rm Tot} = \frac{F_{\rm A} + F_{\rm B}}{I_{\rm A} + I_{\rm B}} \quad (5)$$

where $F_{\rm A,\,B}$ and $I_{\rm A,\,B}$ are, respectively, computed fluxes and continua of each component. The combination of the two spectra has been made after shifting single spectra for the respective observed radial velocity. The simultaneous fitting of Hβ and Hα led to a final solution as the intersection of the two χ^2 iso-surfaces. An important source of uncertainties arises from the difficulties in continuum normalization as it is always challenging for Balmer lines in echelle spectra. We quantified the error introduced by the normalization to be at least 100 K in the effective temperatures discussed below. We summed this error in quadrature with the errors obtained by the fitting procedure.

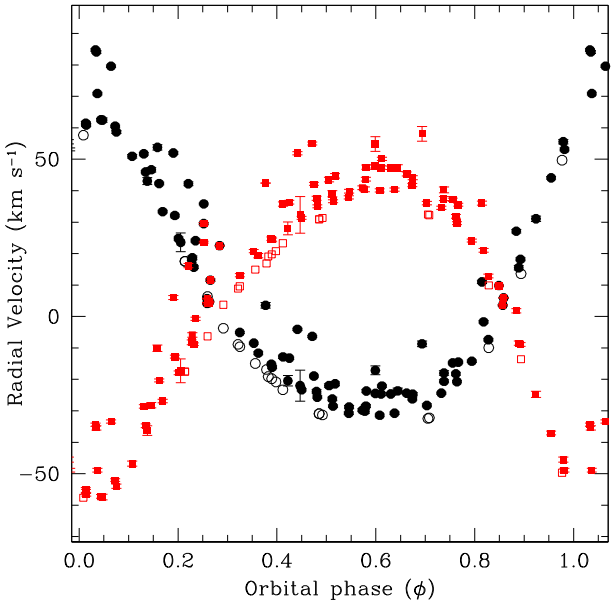

Figure 1. Radial velocities folded with $P(\mathrm{d}) = 31.9080 \pm 0.0006$. Black circles and red squares represent the velocities for the primary and secondary, respectively. In particular filled symbols refer to our data, and open symbols to the Lampens et al. (2018) measurements.

For the determination of effective temperatures and gravities, we used the spectra obtained at the orbital phases $\phi = 0.04$ (HJD = 2458 011.3477) and $\phi = 0.60$ (HJD = 2457 933.5276), when the separation between components A and B was maximum. A grid of atmospheric models has been calculated over the intervals 7000 K $\leq T_{\rm eff} \leq$ 10000 K (step of 100 K) and $3.5 \leq \log g \leq 4.5$ (step of 0.1 dex).

The final results for effective temperatures and gravities are reported in Table 3 and shown in Fig. 5. Uncertainties in $T_{\rm eff}$, $\log g$, and $v \sin i$ as shown in Table 3 were estimated by the changes in parameter values, which lead to increases of χ^2 by unity (Lampton, Margon & Bowyer 1976). Microturbulence velocities have been estimated for both stars by using the calibration given by Gebran et al. (2014). Considering the stars' effective temperatures, we obtained $\xi = 3.1 \pm 0.8$ km s^{-1}.

As a second step we determined the abundances of individual species by spectral synthesis. For this analysis we used the spectrum taken at the HJD = 2458 011.3477 for which the signal-to-noise ratio is the highest we obtained. Therefore, we divided the spectrum into several intervals, 50 Å wide each, and derived the abundances in each interval by performing a χ^2 minimization of the difference between the observed and synthetic composite spectra, computed from single spectra and combined as in equation (5). The minimization algorithm has been written in the *IDL*[1] language, using the *amoeba* routine. We adopted lists of spectral lines and atomic parameters from Castelli & Hubrig (2004), who updated the parameters listed originally by Kurucz & Bell (1995). Errors on abundances have been quantified by combining in quadrature the standard deviation and the uncertainties coming from atmospheric parameters.

[1]IDL (Interactive Data Language) is a registered trademark of Harris Geospatial Solutions.

As an example of result of our procedure, we show in Fig. 6 two spectral regions with, overimposed, the total synthetic spectrum computed by using our results.

The derived abundances for 14 elements are reported in Table 4, while their pattern with respect to the Sun abundances is shown in Fig. 7.

The analysis of Fig. 7 shows clearly underabundances of C, O, Mg, Ca, and Sc, overabundances of Na, iron-peak elements (with exception of Ti, whose abundance is close to the solar value), Zr, and Ba. The sodium abundance has been derived from the Na I doublet at λλ5885–5890 Å. Since these lines are strongly contaminated from both telluric and interstellar sodium lines, the resulting abundances should be considered only as upper limits. In particular, since Ca/Sc and Fe-peak elements are, respectively, lower and higher than the solar abundances, we can confirm that HD 226766 A & B belong to the class of Am stars as reported in Renson & Manfroid (2009).

5 HD 226766 C

So far, we have analyzed observed spectra of HD 226766 neglecting the presence of the C component. By the way, the presence of spectral signatures of the third component has been noted by Lampens et al. (2018). These authors observed broad features in various parts of the spectrum and they attributed those features to a star of spectral type similar to those of the other two components, but more rapidly rotating.

Checking our spectra, we observed an extra broad structure in the spectral region around λ 4481 Å overimposed on the magnesium lines belonging to the A and B components. Assuming that this feature is the line of magnesium generated by HD 226766 C, we have tried to estimate some physical parameters of this star.

Following Catanzaro & Leone (2006), we extend the method applied in Section 4 to include the effect of the third component in the computation of the composite spectrum by using the following formula:

$$F_{\rm Tot} = \frac{F_{\rm A} + F_{\rm B} + F_{\rm C}}{I_{\rm A} + I_{\rm B} + I_{\rm C}} \qquad (6)$$

where $F_{\rm A,B,C}$ and $I_{\rm A,B,C}$ are, respectively, computed fluxes and continua of each component. To derive effective temperatures and gravities of all three components, we fit the same spectra used in the previous section, and obtained the values reported in Table 5. The synthetic profiles of the Hβ and Hα lines are shown in Fig. 8. It is worth noting that, within the experimental errors, effective temperatures and gravities for A and B components are in agreement with those derived neglecting the presence of component C. The rotational velocity of C has been estimated to be $v \sin i = 150 \pm 20$ km s^{-1} by fitting the spectral region centred around λ 4481 Å. Furthermore, by using the same line, we estimated the component C magnesium abundance to be $\log N_{\rm Mg}/N_{\rm tot} = -4.00 \pm 0.2$. The comparison between synthetic and observed spectra is shown in Fig. 9.

With the exception of Mg II λ 4481 Å, we did not observe other evident broad lines in our spectra, so it was not possible to perform a detailed abundance determination for HD 226766 C. This is not a surprise, in fact, due to the high rotational velocity; most lines are shallow and confused at the continuum level. Nevertheless by spectral synthesis we evaluated the error made by neglecting the presence of component C and we concluded that we have underestimated metal abundances by a factor up to 0.5 dex.

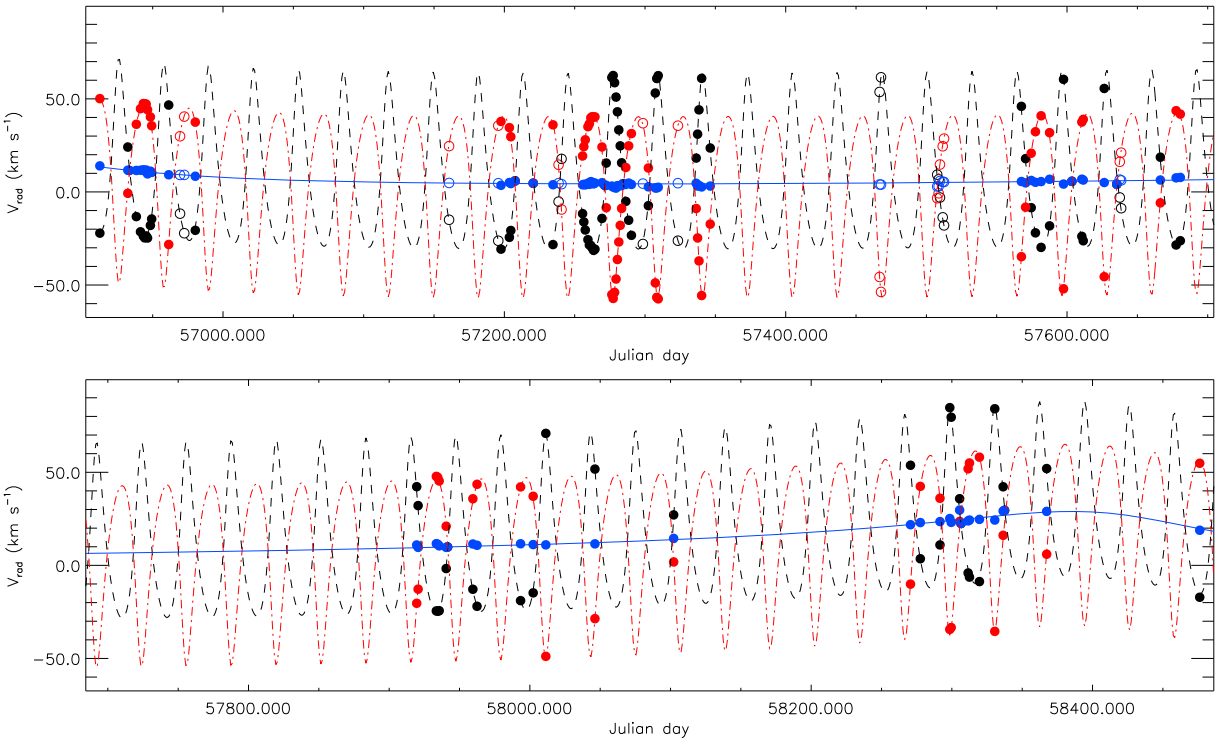

Figure 2. Radial velocities for the three components of HD 226766 as a function of heliocentric julian day. Black, red, and blue dots represent velocities for primary, secondary, and centre of mass, respectively. Filled symbols are velocities derived from CAOS spectroscopy, while open symbols are those from Lampens et al. (2018). Theoretical curves, computed with the orbital parameters reported in Table 2, are overimposed, in particular black dashed line is for the primary, red dot-dashed for the secondary, and solid blue line for the motion of the centre of mass.

Table 2. Parameters derived through modeling radial velocity curves the SB2 A&B couple (upper table) and for the A&B + C system (lower table).

	A		B
JD_0			
		58 488.931 ± 0.003	
P (days)		31.9187 ± 0.0001	
e		0.28 ± 0.01	
ω		338° ± 1°	
γ (km s^{-1})		(var)	
K (km s^{-1})	47.31 ± 0.07		48.81 ± 0.07
$a\sin i$ ($R_\odot$)	28.6 ± 0.1		29.5 ± 0.1
$M\sin^3 i$ ($R_\odot$)	1.49 ± 0.03		1.44 ± 0.03
M_A/M_B		1.03 ± 0.03	

C	
JD_0	58417 ± 24
P (days)	1615 ± 59
e	0.54 ± 0.11
ω	28° ± 5°
γ (km s^{-1})	10.8 ± 0.5
K (km s^{-1})	12.3 ± 0.7
$a\sin i$ ($R_\odot$)	329 ± 43
$f(m)$ ($M_\odot$)	0.18 ± 0.07

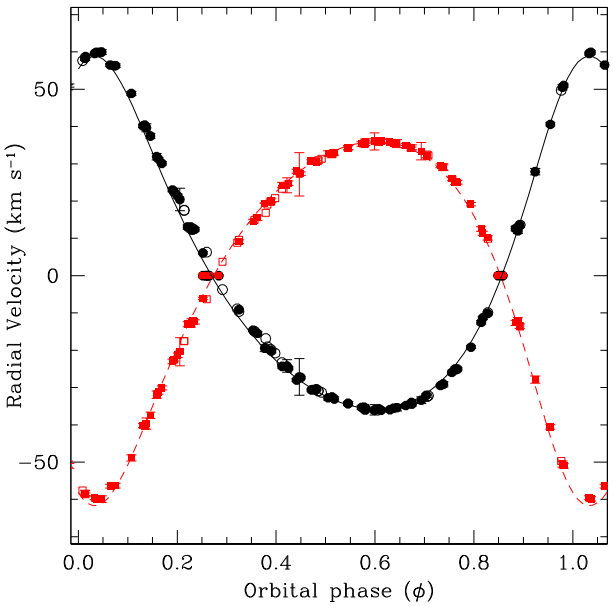

Figure 3. Radial velocities for the inner SB2 system folded with orbital parameters reported in Table 2. Symbols are as in Fig. 2.

6 DISCUSSION AND CONCLUSIONS

In this paper, by means of our high-resolution spectra obtained at the 91 cm telescope of the Catania Astrophysical Observatory equipped with the CAOS spectrograph, we presented a detailed spectroscopic study of the SB3 system HD 226766. Our spectra have been used for two purposes: (i) to solve the orbits both of the inner pair and

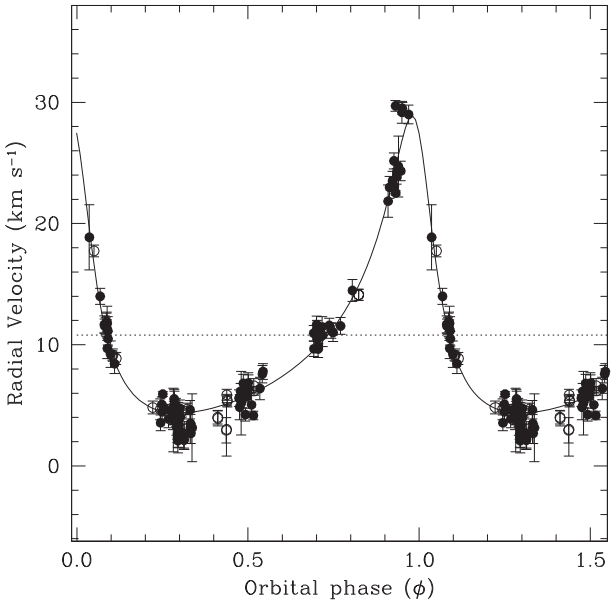

Figure 4. Radial velocities for the mass centre of the inner binary folded with orbital parameters reported in Table 2. Filled symbols refer to radial velocity obtained from CAOS spectroscopy, while open dots refer to the Lampens et al. (2018) measurements.

Table 3. Effective temperatures, surface gravities, and projected rotational velocities for both components of the inner HD 226766 system.

	A	B
$T_{\rm eff}$ (K)	8600 ± 500	8500 ± 400
$\log g$	3.8 ± 0.2	4.0 ± 0.2
$v\sin i$ (km s^{-1})	13 ± 1	13 ± 1

outer component and (ii) to investigate the chemical composition of the components to confirm if there is any peculiarity.

Regarding orbital solution, for the inner pair we found $P = 31.9187 \pm 0.0001$ d, $e = 0.28 \pm 0.01$, and a mass ratio $M_{\rm A}/M_{\rm B} = 1.03 \pm 0.03$, while the outer component orbits with a long period of $P = 1615 \pm 59$ d around the inner pair in a very eccentric orbit with $e = 0.54 \pm 0.11$ and has a mass function $f(m) = 0.18 \pm 0.07$ M$_\odot$.

We determined atmospheric parameters for the inner pair, including effective temperatures, gravities, rotational velocities, and chemical abundances. According to our spectroscopic analysis, both components are almost twin main sequence stars with $T_{\rm eff} = 8600 \pm 500$ K and $\log g = 3.8 \pm 0.2$ for HD 226766 A and $T_{\rm eff} = 8500 \pm 400$ K and $\log g = 4.0 \pm 0.2$ for HD 226766 B (spectral type approximately A4 V). From our analyses of chemical pattern, the A & B components show underabundances of carbon, oxygen, magnesium, calcium, and scandium (up to 2 dex), close to solar abundances for silicon and titanium, and overabundances for sodium, iron-peak, and heavy elements.

Considering, in particular, underabundances of calcium and scandium and overabundance of iron-peak elements, we conclude that both A and B components are Am stars.

In this study we tried to evaluate some physical properties of HD 226766 C and its influence on the results obtained for A and B components. In particular, by spectral synthesis of Hβ and Hα lines, we obtained that HD 226766 C is a main sequence ($\log g = 4.0$) rapidly rotating ($v\sin i = 150 \pm 20$ km s^{-1}) star with $T_{\rm eff} = 8000 \pm 500$ K. From its magnesium line Mg II λ 4481 Å, we derived an overabundance of ≈ 0.5 dex. Unfortunately no other spectral lines are visible in our spectra. Neglecting the presence of the third component, we underestimated abundances of A and B components by a factor up to 0.5 dex.

Since all the components have, within the errors, the same effective temperatures, we can adopt for all of them the same value for masses, that is about 2 M$_\odot$ (Cox 2000). With this hypothesis we estimated the inclination angles for both inner and outer orbits of the system. For the inner pair, following the results of $M\sin^3 i$ (see Table 2), we obtained $i = (47 \pm 1)^\circ$, while for the outer orbit

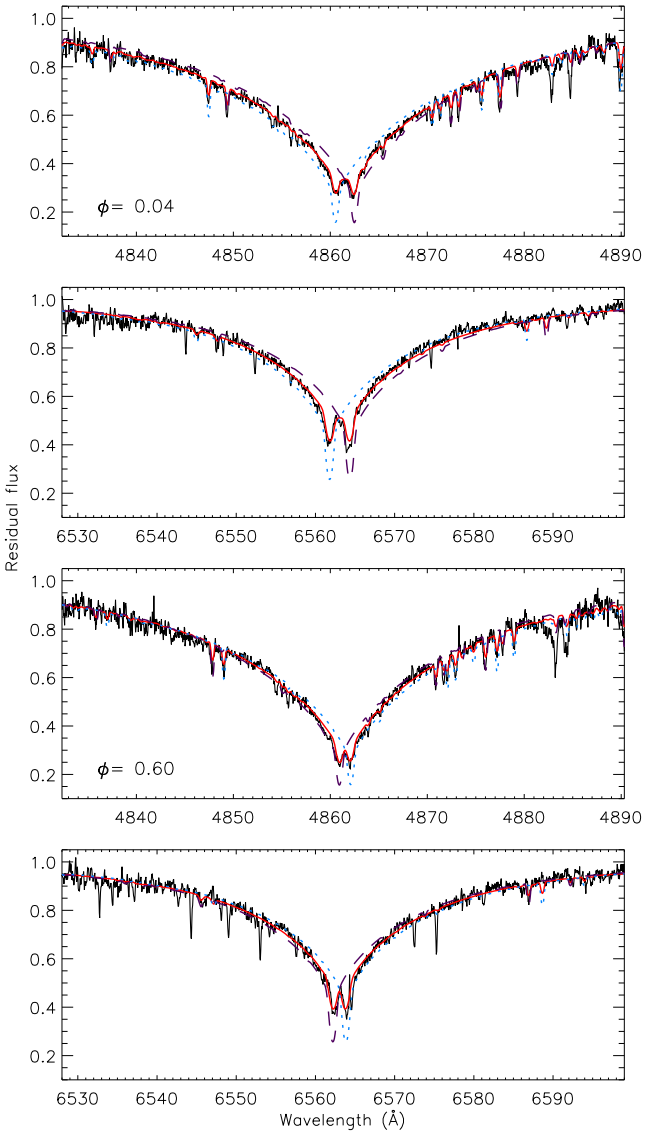

Figure 5. Balmer lines H$_\beta$ and H$_\alpha$ observed at two different orbital phases corresponding at the maximum of radial velocity curve. For each line, overimposed to the observed spectra, we show the synthetic spectra for the A component (cyan) and the B component (violet), plus the composite theoretical spectra. The top panels represent H$_\beta$ and H$_\alpha$ at orbital phase 0.04 and the lower two panels the same lines at orbital phase 0.60.

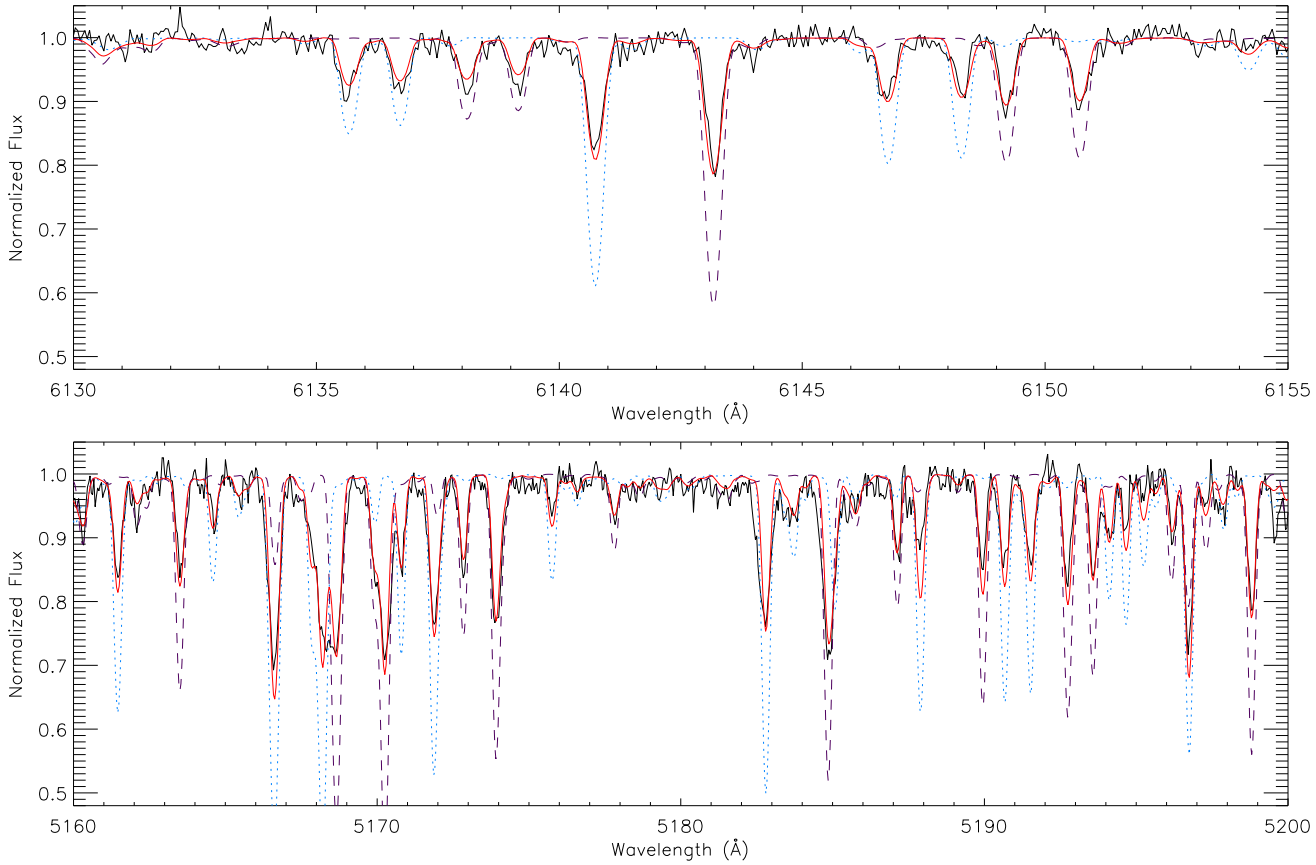

Figure 6. Observed spectrum of HD 226766 (black line) with overimposed composite synthetic spectrum (red line), synthetic spectra for primary (cyan dotted line) and for secondary (violet dashed line). Synthetic spectra have been computed as described in the text.

Table 4. Abundances derived for HD 226766 A & B components. Values are expressed in the form $\log N_{\rm el}/N_{\rm tot}$. The abundances of carbon and scandentium have to be considered only as upper limits.

Element	A	B
C	≤ -4.5	≤ -4.5
O	-3.8 ± 0.1	-3.8 ± 0.1
Na	-4.0 ± 0.1	-5.3 ± 0.1
Mg	-5.2 ± 0.2	-4.7 ± 0.1
Si	-4.4 ± 0.2	-4.3 ± 0.2
Ca	-6.0 ± 0.1	-6.0 ± 0.1
Sc	≤ -11.0	≤ -11.0
Ti	-7.0 ± 0.1	-7.0 ± 0.1
Cr	-5.7 ± 0.2	-5.3 ± 0.2
Fe	-4.0 ± 0.2	-4.1 ± 0.1
Ni	-4.9 ± 0.1	-4.9 ± 0.1
Sr	-8.9 ± 0.1	-8.9 ± 0.1
Zr	-8.0 ± 0.1	-8.4 ± 0.1
Ba	-7.7 ± 0.1	-7.7 ± 0.1

considering the mass function defined as

$$f(m) = \frac{M_2^3 \sin^3 i}{(M_1 + M_2)^2} \tag{7}$$

and the results reported in Table 2 we derived $i = (54 \pm 19)^\circ$. Considering the errors on the angles, the coplanarity of the inner and outer orbits is a possible option, making this triple system more interesting from the evolutionary point of view. To better constrain

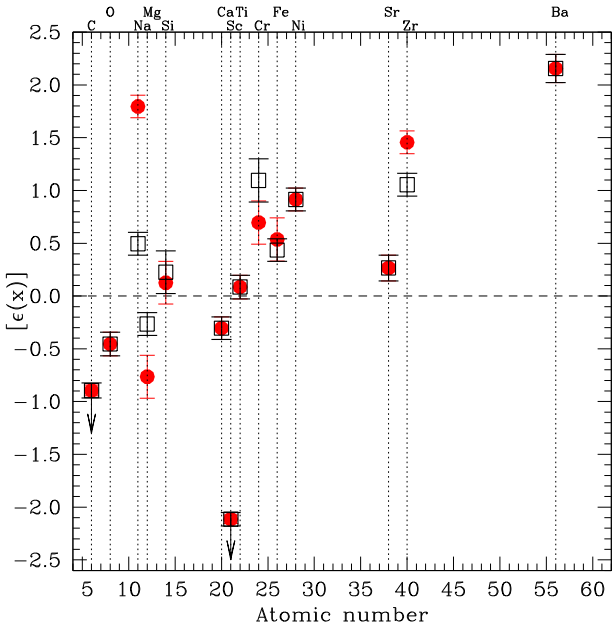

Figure 7. Chemical pattern for HD 226766 A (red dots) and HD 226766 B (open squares). Horizontal dashed line corresponds to solar abundances (Grevesse et al. 2010). Since abundances of carbon, sodium, and scandium are only upper limits, errorbars have been replaced by arrows.

Table 5. Effective temperatures and surface gravities for all components of the HD 226766 system.

	A	B	C
$T_{\rm eff}$ (K)	8700 ± 500	8700 ± 400	8000 ± 500
$\log g$	4.0 ± 0.2	4.1 ± 0.2	4.0 ± 0.3

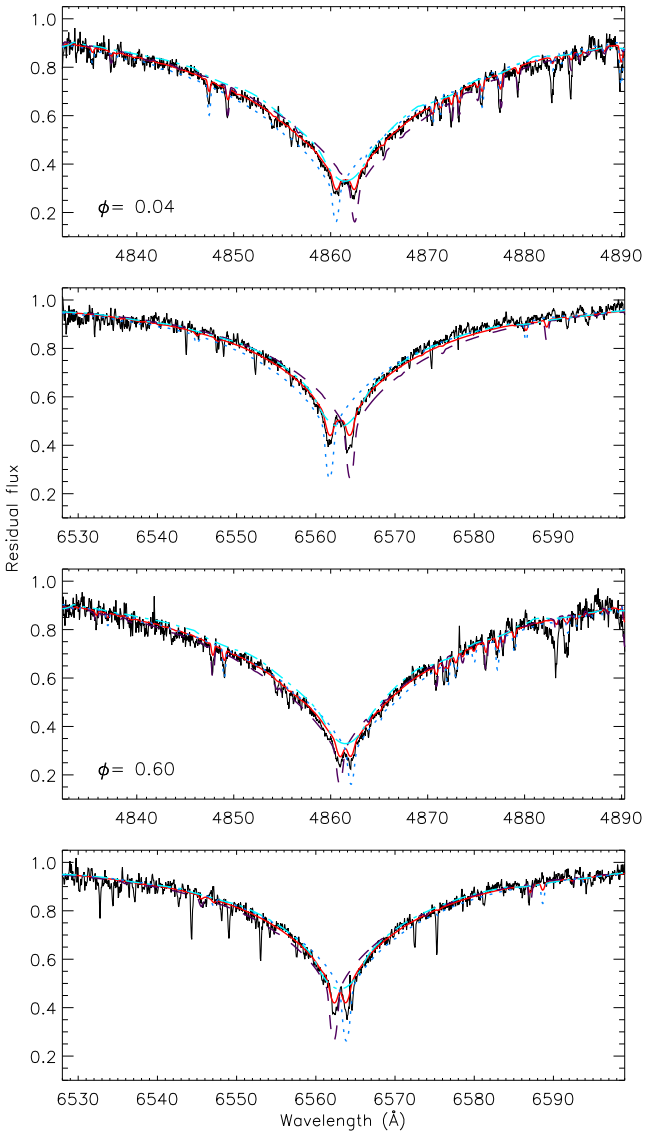

Figure 8. As in Fig. 5 but considering also the Balmer lines for HD 226766 C (cyan dot-dashed line).

the outer inclination angle, we need to improve the solution for the third component, so more observations are needed.

ACKNOWLEDGEMENTS

This study is based on observations made with the Catania Astrophysical Observatory Spectropolarimeter (CAOS) operated by the Catania Astrophysical Observatory.

This research has made use of the SIMBAD database and VizieR catalogue access tool, operated at CDS, Strasbourg, France.

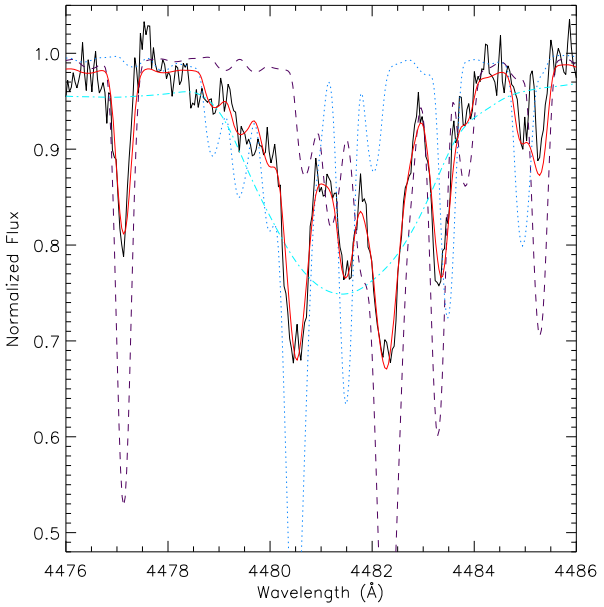

Figure 9. Observed spectrum centred around spectral region containing the Mg II λ4481 Å (taken at HJD = 2458 011.3477) with overimposed composite synthetic spectrum. Meaning of the lines is as in Fig. 6, with the exception of cyan dot-dashed line that represents the synthetic spectrum of the tertiary component.

REFERENCES

Castelli F., Hubrig S., 2004, A&A, 425, 263
Catanzaro G., 2010, A&A, 509A, 21
Catanzaro G., 2017, 'Studies of close binary systems triggered by the LAMOST-Kepler survey', presented at the '2nd LAMOST-Kepler workshop. LAMOST in the era of large spectroscopic surveys', held on July 31–August 3, 2017 at the Royal Observatory of Belgium, Bruxelles. Available at: http://events.oma.be/indico/event/26/session/11/contribution/79
Catanzaro G., Balona L. A., 2012, MNRAS, 421, 1222
Catanzaro G., Leone F., 2006, MNRAS, 373, 330
Catanzaro G., Ripepi V., 2014, MNRAS, 441, 1669
Catanzaro G., Ripepi V., Bruntt H., 2013, MNRAS, 431, 3258
Catanzaro G., Ripepi V., Biazzo K., et al., 2015, MNRAS, 451, 184
Catanzaro G., Busá I., Gangi M., Giarrusso M., Leone F., Munari M., 2019, MNRAS, 484, 2530
Cox A. N., 2000, in Cox A. N., ed., Allen's Astrophysical qQuantities, 4th edn., AIP Press; Springer, New York
De Cat P. et al., 2015, ApJS, 220, 19
Frasca A., Molenda-Zakowicz J., De Cat P. et al., 2016, A&A, 594A, 39
Gebran M., Monier R., Royer F., Lobel A., Blomme R., 2014, in Mathys G., Griffin E., Kochukhov O., Monier R., Wahlgren G., eds, 'Putting A Stars into Context: Evolution, Environment, and Related Stars', Proceedings of the international conference held on June 3-7, 2013 at Moscow M.V. Lomonosov State University in Moscow, Russia. 'Pero', Moscow, p. 193
Grevesse N., Asplund M., Sauval A. J., Scott P., 2010, Ap&SS, 328, 179
Kurucz R. L., Bell B., 1995, Kurucz CD-ROM No. 23. Cambridge, USA
Kurucz R. L., 1993, Kurucz CD-ROM 13: ATLAS9. SAO. Cambridge, USA
Kurucz R. L., 1993, in Dworetsky M. M., Castelli F., Faraggiana R., eds, A new opacity-sampling model atmosphere program for arbitrary abundances. In: Peculiar versus Normal Phenomena in A-type and Related Stars, IAU Colloquium 138, ASP Conf. Ser. Vol. 44. Astronomical Society of the Pacific, San Francisco, CA, p. 87

Kurucz R. L., Avrett E. H., 1981, SAO Special Rep. Smithsonian Astrophysical Observatory, Cambridge, Massachusetts (USA), p. 391
Lampens P., Frémat Y., Vermeylen Á., De Cat P., Dumortier L., Sodor A., Sharka M., Bognar S., 2018, A&A, 610, 17
Lampton M., Margon B., Bowyer S., 1976, ApJ, 208, 177
Leone F., Catanzaro G., 1999, A&A, 343, 273
Leone F. et al., 2016, AJ, 151, 116
Murphy S. J., Bedding T. R., Shibahashi H., Kurtz D. W., Kjeldsen H., 2014, MNRAS, 441, 2515
Murphy S. J., Maxwell M., Kurtz D. W., Bedding T. R., Shibahashi H., Boffin H. M. J., 2018, MNRAS, 474, 4322
Press W. H., Teukolsky S. A., Vetterling W. T., Flannery B. P., 1992, Numerical Recipes in Fortran. 2nd edn., Cambridge Univ. Press, Cambridge
Renson P., Manfroid J., 2009, A&A, 498, 961
Stellingwerf R. F., 1978, ApJ, 224, 953

This paper has been typeset from a TEX/LATEX file prepared by the author.